Observational evidence for AGN feedback in early-type galaxies

Kevin Schawinski,[1]* Daniel Thomas,[1,2] Marc Sarzi,[1,3] Claudia Maraston,[1,2]
Sugata Kaviraj,[1] Seok-Joo Joo,[4] Sukyoung K. Yi[4] and Joseph Silk[1]

[1]*Department of Physics, University of Oxford, Oxford OX1 3RH*
[2]*Institute of Cosmology & Gravitation, University of Portsmouth, Portsmouth PO1 2EG*
[3]*Centre for Astrophysics Research, Science & Technology Research Institute, University of Hertfordshire, Hatfield AL 10 9AB*
[4]*Centre for Space Astrophysics, Yonsei University, Seoul 120-749, Korea*

ABSTRACT

A major amendment in recent models of hierarchical galaxy formation is the inclusion of so-called active galactic nucleus (AGN) feedback. The energy input from an active central massive black hole is invoked to suppress star formation in early-type galaxies at later epochs. A major problem is that this process is poorly understood, and compelling observational evidence for its mere existence is still missing. In search for signatures of AGN feedback, we have compiled a sample of 16 000 early-type galaxies in the redshift range $0.05 < z < 0.1$ from the Sloan Digital Sky Survey (SDSS) data base (MOSES: Morphologically Selected Ellipticals in SDSS). Key in our approach is the use of a purely morphological selection criterion through visual inspection which produces a sample that is not biased against recent star formation and nuclear activity. Based on the nebular emission-line characteristics we separate between star formation activity, black hole activity, the composite of the two and quiescence. We find that emission is mostly LINER (low ionization nuclear emission line region) like in high-mass galaxies ($\sigma > 200 \, \mathrm{km \, s^{-1}}$) and roughly evenly distributed between star formation and AGN at intermediate and low ($\sigma < 100 \, \mathrm{km \, s^{-1}}$) masses. The objects with emission ($\sim$20 per cent) are offset from the red sequence and form a well-defined pattern in the colour–mass diagram. Star-forming early-types inhabit the blue cloud, while early-types with AGN are located considerably closer to and almost on the red sequence. Star formation–AGN composites are found right between these two extremes. We further derive galaxy star formation histories using a novel method that combines multiwavelength photometry from near-ultraviolet (UV) to near-infrared (IR) and stellar absorption indices. We find that in those objects deviating from the red sequence star formation occurred several 100 Myr in the past involving 1–10 per cent of the total stellar mass. We identify an evolutionary sequence from star formation via nuclear activity to quiescence. This transition process lasts about 1 Gyr, and the peak AGN phase occurs roughly half a Gyr after the starburst. The most likely interpretation is that star formation is suppressed by nuclear activity in these objects before they settle on the red sequence. This is empirical evidence for the occurrence of AGN feedback in early-type galaxies at recent epochs.

Key words: galaxies: active – galaxies: elliptical and lenticular, cD – galaxies: evolution – galaxies: formation.

1 INTRODUCTION

The formation of early-type galaxies is one of the major unsolved problems of astrophysics. Despite their apparent simplicity, they have time and again refused to fit into the bigger picture and thus, they have been the most difficult and illuminating test for galaxy and structure formation theory. In every generation of theoretical models, early-type galaxies have helped provide the insights into what physics was still missing from them and they continue to do so. The vast majority of early-type galaxies appear to have formed most of their stars at high redshift on very short time-scales as suggested by the stellar population properties of nearby samples (e.g. Trager et al. 2000; Nelan et al. 2005; Thomas et al. 2005; Bernardi et al. 2006; Jimenez et al. 2006) as well as the redshift evolution of luminosity and mass functions of massive galaxies

---

*E-mail: kevins@astro.ox.ac.uk

(e.g. Cimatti, Daddi & Renzini 2006; Wake et al. 2006; Rodighiero et al. 2007b).

Until very recently, the predictions from semi-analytic models of hierarchical galaxy formation were in severe conflict with the observationally derived formation ages and time-scales of early-type galaxies. These models take the merger trees of dark matter haloes in a Λ cold dark matter (ΛCDM) universe either by following them in a cosmological *N*-body simulation (Kauffmann et al. 1999) or generating them using the extended Press–Schechter formalism (White & Frenk 1991). They then calculate the more complex fate of baryonic matter inside them with prescriptions for star formation (SF; Kennicutt 1998), radiative cooling of gas (Sutherland & Dopita 1993; Springel et al. 2001) and feedback from supernovae (Kauffmann et al. 1999). Early semi-analytic models such as that of Kauffmann & Charlot (1998) predicted that the most massive galaxies in the universe harbour the youngest stellar populations and assemble the last, contrary to what has been deduced from observations. For a critical example, these models struggle to match the observed chemical abundance ratios and their trends with galaxy mass (Thomas 1999; Nagashima et al. 2005).

The reason for this failure in the early models is that SF continues unchecked in massive haloes where supernova feedback is insufficient (Dekel & Silk 1986). Benson et al. (2003) showed that in massive galaxies, an additional, more powerful heating source than supernovae is needed to heat the cold gas that fuels SF and therefore stop it. This additional heating source is now generally identified as feedback from active galactic nuclei (AGN) where jets and outflows from the central supermassive black hole are presumed to heat and expel most residual gas via a wind thus preventing further SF. This AGN feedback has been discussed by a number of authors (Ciotti & Ostriker 1997; Silk & Rees 1998; Binney 2004; Silk 2005; Springel, Di Matteo & Hernquist 2005a) and is now part of many galaxy formation models (Granato et al. 2001, 2004; Kaviraj et al. 2005; Kawata & Gibson 2005; Springel et al. 2005b; Bower et al. 2006; Cattaneo et al. 2006, 2007; Croton et al. 2006; De Lucia et al. 2006; Cavaliere & Menci 2007). The phenomenological model of Schawinski et al. (2006a) is specifically motivated by Galaxy Evolution Explorer (GALEX) observations of early-type galaxies. Di Matteo, Springel & Hernquist (2005) and Springel et al. (2005a) have also investigated the effect of AGN feedback in hydro simulations of mergers and have now placed them in large-scale simulations probing cosmological volumes (Di Matteo et al. 2007; Sijacki et al. 2007). Note that alternatives have been suggested based on the processes of cooling and shock heating of baryonic matter in dark matter haloes (Birnboim, Dekel & Neistein 2007; Hopkins et al. 2007; Khochfar & Ostriker 2007).

AGN feedback may come in two different modes at different epochs during cosmic time. In an early phase at high redshifts the AGN may truncate and quench SF leading to the formation of the dominant old population in massive galaxies. This so-called 'quasar mode' (Croton et al. 2006) is most likely accompanied by vigorous black hole growth and leads to very strong kinetic feedback that quenches strong starbursts. The other face of AGN feedback can be thought of as a 'maintenance' mode. It turns on at more recent epochs such that further significant episodes of SF are prevented (Best et al. 2005, 2006; Fabian et al. 2005, 2006). The coupling between the black hole accretion and the gas heating is poorly constrained by the observation. The latter mechanism has only recently been included in semi-analytic galaxy formation models. While such prescriptions are successful at curing some key issues, their major problem is that the physics of this process is still poorly understood and essentially unconstrained by observations. Compelling observational evidence for the mere existence of AGN feedback in early-type galaxies is still missing.

The aim of this paper is to tackle the key question of the role of AGN feedback observationally by looking for its signatures in early-type galaxies at recent epochs in the nearby universe. Crucial for this purpose is the compilation of a sample of early-type galaxies with a selection method that does not bias against AGN and/or SF. The sample further needs to be large, because the potentially short duration of the AGN feedback phase makes such objects relatively rare. To this end we have constructed a sample of nearly 16 000 early-type galaxies from the Sloan Digital Sky Survey (SDSS) in the redshift range $0.05 \leqslant z \leqslant 0.1$. These early-types are part of a sample comprising 50 000 early- and late-type galaxies in that redshift range compiled in a project called Morphologically Selected Ellipticals in SDSS (MOSES; Schawinski et al., in preparation). The major novelty is the purely morphological selection mechanism through visual inspection of all 50 000 galaxies. Through emission line diagnostics we identify active early-type galaxies with SF activity and/or AGN. From the stellar populations we derive SF histories for these objects, which allows us to explore the possible interaction between the formation histories of the galaxies and their current SF/AGN activities.

The paper is organised as follows. In Sections 2 and 3, we outline the sample selection, present the emission-line diagnostics and the stellar population analysis. We place the sample galaxies subdivided in quiescent, AGN and star forming objects on the colour–σ relation and discuss first tentative conclusions in Section 4. A more quantitative discussion is provided in Section 5 based on the two-component SF histories derived. Conclusions in the context of AGN feedback in galaxy formation are discussed in Sections 6 and 7.

Throughout this paper, we assume a standard ΛCDM cosmology consistent with the *WMAP* (*Wilkinson Microwave Anisotropy Probe*) results (Bennett et al. 2003) with $\Omega_m = 0.3$, $\Omega_\Lambda = 0.7$ and $H_0 = 70\,h_{70}\,\mathrm{km}^{-1}\,\mathrm{s}^{-1}$. All magnitudes are in the AB system.

2 DATA SAMPLE

The sample utilized here is part of a project called MOSES. Key is that all 48 023 galaxies in this sample have been visually inspected and classified into early- and late-type morphology by eye, yielding a sample of 15 729 early-type galaxies. A detailed description of the catalogue can be found in a companion paper (Schawinski et al., in preparation), and we refer the reader to this paper for any details. In the following, we provide a brief summary with focus on the aspects that are most relevant for the present work.

2.1 Sample selection

We use the SDSS Data Release 4 (DR4) as our main sample (York et al. 2000; Stoughton et al. 2002; Adelman-McCarthy et al. 2006). The SDSS is a survey of the northern sky providing us with photometry in the five filters *u,g,r,i* and *z* (Fukugita et al. 1996; Gunn et al. 1998). We selected objects from the redshift slice $0.05 < z < 0.10$ with the magnitude limit $r < 16.8$. These cuts are mostly motivated by the limit out to which a visual inspection of galaxy morphology is reliable (see Schawinski et al. 2006b).

2.2 Morphological classification

The selection criteria used to identify early-type galaxies are crucial. Selection criteria based on galaxy properties such as colour, spectral features or concentration index rather than morphology are at risk

to be biased against early-type galaxies with residual SF or AGN activity. As these are the objects most relevant for the present study, we decided for a radical, purely morphological selection.

The first catalogues of early-type galaxies in the SDSS used for extensive study are those of Eisenstein et al. (2001) and Bernardi et al. (2003a,b,c,d). The Bernardi et al. (2003a) catalogue is based primarily in the likelihood of the surface-brightness profile resembling a de Vaucouleurs law and a high concentration index. This is a very efficient way of selecting large numbers of spheroids, but can fail to reject spiral galaxies with prominent bulges. In particular, spirals with face-on faint discs and edge-on discs can pass these criteria. Furthermore, Bernardi et al. (2003a) reject galaxies with a principal component analysis (PCA) classification number atypical of red, passive early types (Connolly & Szalay 1999). This means that early types with strong emission lines or that are dominated by young stellar populations are rejected despite having early-type morphology. For an example, the early-type galaxies discussed by Fukugita et al. (2004) would not be included. Recently, Fukugita et al. (2007) have compiled an catalogue of morphological early-type galaxies by visual inspection of 2658 objects from the SDSS.

For the MOSES sample we carried out manual inspection of multicolour images from SDSS by eye for all 48 023 galaxies, in order to avoid any potential bias introduced by selecting by colours or spectral features. We define as early-type galaxies all objects earlier than and including S0 galaxies and reject galaxies from our sample if they show distinct spiral arms or a disc. We include in this selection objects with clear tidal features or other signs of morphological disturbance. In the paper presenting the MOSES catalogue (Schawinski et al., in preparation) we present a number of example images from SDSS to illustrate the effectiveness of our visual inspection. Out of the 48,023 galaxies in our volume-limited sample, we identify 15 729 early-type galaxies. Fig. 1 illustrates the difference between our selection and that of Bernardi et al. (2003a) in the colour–σ diagram. It can be seen clearly that our morphological selection yields a significantly higher fraction of early-type galaxies with emission lines and/or blue colours. Less than 5 per cent of the early-type galaxies in the catalogue of Bernardi et al. (2003a) show emission lines, while over 18 per cent of ours do.
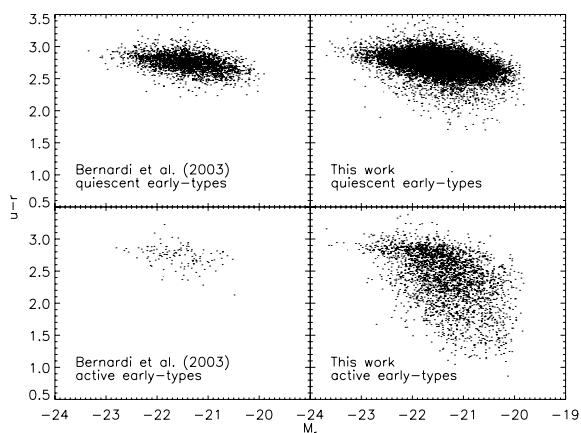

Figure 1. Optical colour–magnitude relation for the early-type catalogue of Bernardi et al. (2003a) and this work. Early-type galaxies are divided into 'quiescent' and 'active' depending on whether emission lines are detected. Our purely morphologically selected sample contains a significantly larger fraction of active early-type galaxies.

2.3 Photometry

We retrieved SDSS model magnitudes (*modelMag*) for all five filters *u,g,r,i* and *z* from the SDSS DR4 data base. In order to improve the wavelength coverage of the galaxies in our sample, we match them to a number of other surveys, namely GALEX, 2MASS (Two Micron All Sky Survey) and SWIRE (*Spitzer* Wide Area Infrared Extragalactic Survey).

2.3.1 Matching to GALEX

The GALEX (Martin et al. 2005) is conducting several surveys of the ultraviolet sky in two filters: far-UV (FUV; 1344–1786 Å) and near-UV (NUV; 1771–2831 Å). The Medium Imaging Survey from the General Release 3 (MIS/GR3) is covering a portion of the sky coinciding with the SDSS to a limit of 23 AB in NUV and FUV. We match our galaxies to MIS within 4 arcsec to find counterparts. GR3 only covers a fraction of SDSS DR4 and so this matching gives us detections for 13.4 per cent of galaxies.

2.3.2 Matching to 2MASS

The 2MASS (Skrutskie et al. 2006) provides us with *J, H* and K_s band imaging for our galaxies selected in SDSS. We match our galaxies to the Extended Source Catalogue (XSC) within 4 arcsec, giving us counterparts for 87.1 per cent. The 2MASS photometry is done in the Vega system, so in order to keep consistency with the rest of the MOSES sample, we convert the magnitudes from Vega to AB following Blanton et al. (2003b, 2005).

2.3.3 Matching to Spitzer-SWIRE

The SWIRE (Lonsdale et al. 2003) is one of the *Spitzer* Legacy Surveys and imaged nearly 50 deg² using both the Infrared Array Camera (IRAC; 3.6, 4.5, 5.8, 8.0 µm) and Multiband Imaging Photometer for *Spitzer* (MIPS; 24, 70, 160 µm) instruments. We cross-match the MOSES sample to the public source catalogues for ELAIS N1, N2 and Lockman Hole fields. Only a small fraction of our sample (0.3 per cent) has counterparts at 3.6 µm.

2.4 Spectroscopy

SDSS has performed follow-up spectroscopy using 3-arcsec fibres yielding a reasonably complete sample to $r < 17.77$ (Blanton et al. 2003a). The spectra cover the range of 3800 to 9200 Å at a resolving power of 1800 and for the MOSES sample have a typical signal-to-noise ratio (S/N) of about 30. We retrieve the SDSS optical spectra for all our galaxies.

2.4.1 Gas and stellar kinematics

We measure the kinematics of the stars and the emission-line fluxes of our galaxies from their SDSS spectra following the methods of Cappellari & Emsellem (2004) and Sarzi et al. (2006), respectively.[1] We separate the contribution of the stellar continuum and of the ionized-gas emission to the observed galaxy spectrum by fitting simultaneously stellar population templates (from Tremonti et al. 2004) and Gaussian emission-line templates to the data. In these fits

---

[1] We made use of the corresponding PPXF and GANDALF IDL (Interactive Data Language) codes adapted for dealing with SDSS data. Both softwares can be retrieved at http://www.strw.leidenuniv.nl/sauron/
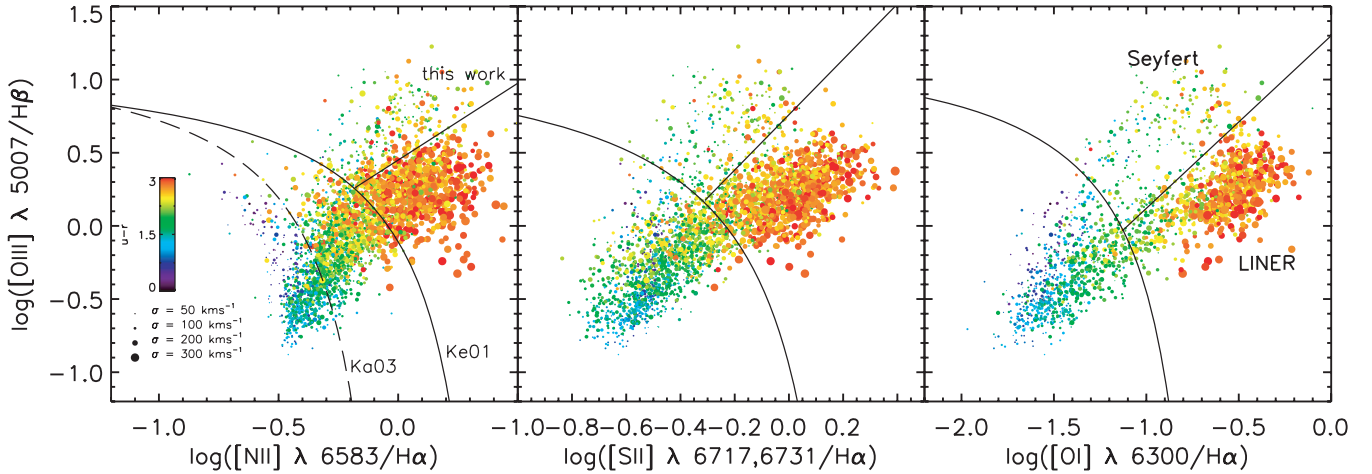
Figure 2. The BPT line diagnostic diagrams for the early-type galaxies of the MOSES sample. Each galaxy is coloured by its optical $u - r$ colour (see colour bar in left-hand panel). Point sizes scale with the galaxy velocity dispersion as an indicator of mass (see legend in left-hand panel). In each diagram, we indicate the demarcation lines used in our classification scheme. The dashed line in the [N II]/Hα diagram (left-hand panel) is the empirical SF line of Kauffmann et al. (2003) (labelled Ka03), while the solid curve (in all three panels) is the theoretical maximum starburst model from Kewley et al. (2001) (labelled Ke01). The galaxies in between these two lines are SF–AGN composites or 'transition region objects'. Galaxies below the Ka03 line are dominated by SF. The division line between Seyferts and LINERs is shown as the straight line following Kewley et al. (2006) for the middle and right-hand panel and our own definition (see text) for the left-hand panel.

we account also for the impact of diffuse dust in the galaxy of dust in the emission-line regions, which allows to obtain a decrement on the strength of the Balmer lines that is at least what expected by recombination theory. From the fit to the stellar continuum and absorption features, we measure the line-of-sight velocity dispersions. From subtraction of the emission-line spectrum from the observed one, we get the clean absorption line spectrum free from emission-line contamination. We then use this cleaned spectrum to measure the stellar absorption indices. The physical constraints on the emission from high-order Balmer lines ensures the strength of the corresponding absorption features is correctly estimated, which is crucial for constraining the ages of stellar populations.

2.4.2 Lick absorption line indices

On each spectrum we measure the 25 standard Lick absorption line indices (Worthey et al. 1994; Worthey & Ottaviani 1997) following the most recent index definitions of Trager et al. (1998). For this purpose the spectral resolution is reduced to the wavelength-dependent Lick resolution (Worthey & Ottaviani 1997). The measurements are then corrected for velocity dispersion broadening. The correction factor is evaluated using the best-fitting stellar template and velocity dispersion obtained previously. Errors are determined by Monte Carlo simulations on each spectrum individually based on the S/N provided by the SDSS. Possible discrepancies between the flux-calibrated SDSS spectral system and the Lick system are negligible, as shown in a detailed analysis of Lick standard stars observed with SDSS (Carson 2007).

2.5 Emission-line diagnostics

Emission-line diagnostic diagrams are a powerful way to probe the nature of the dominant ionizing source in galaxies (Baldwin, Phillips & Terlevich 1981, hereafter BPT). They allow the separation of galaxies into those dominated by ongoing SF and non-stellar processes; and with sufficient information can further split those into

Seyfert AGN and LINERs (low ionization nuclear emission line regions). The diagrams also contain a transition region, where the emission lines indicate a blend of SF and AGN activity.

We use the four optical line ratios [O III] λ5007/Hβ, [N II] λ6583/Hα, [S II] λ6717/Hα and [O I] λ6300/Hα. We follow the S/N criterion of Kauffmann et al. (2003) and classify all galaxies that have a S/N > 3 detection of Hα, Hβ, [O III] λ5007 and [N II] λ6583. The two low ionization species [S II] and [O I] are used when detected, as they are usually weaker than the other four.

2.5.1 Diagnostic diagrams

The corresponding three diagnostic diagrams are shown in Fig. 2. Each galaxy is coloured by its optical $u - r$ colour. Point sizes scale with the galaxy velocity dispersion as an indicator of mass. In each diagram, we indicate the demarcation lines used in our classification scheme. In the left-hand column, we show the [N II]/Hα diagram used to separate star-forming objects (blue) by means of the demarkation line by Kauffmann et al. (2003, dashed line). We verified that the somewhat more restrictive separation between star forming and AGN suggested by Stasińska et al. (2006) does not alter the results of this work. The remaining objects are divided in composite transition region objects (purple) and AGN using the theoretical maximum starburst model from Kewley et al. (2001, solid lines).

The AGN are then further subclassified into Seyferts (green) and LINERs (red) by the straight solid lines. The more indicative low ionization species (middle and right-hand panel) are used where possible. The best separation of Seyferts and LINERs is achieved using [O I] (right-hand panel of Fig. 2), which is used wherever [O I] is detected with S/N > 3. The [O I] line is generally weaker then any of the other emission lines used, so where it is not available, we use [S II]. To separate the two types of AGN, we use the lines defined by Kewley et al. (2006). If both these lines are not detected we adopt the original [N II] diagram for AGN classification. Based on the location of those galaxies classified by [O I] or [S II]
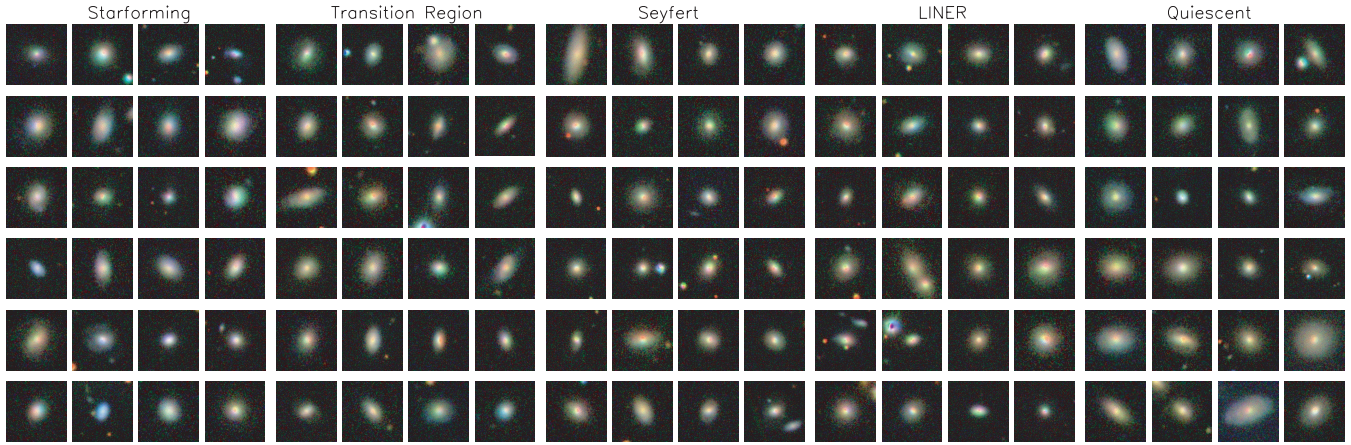
Figure 3. A sample of morphological early-type galaxies from the MOSES sample sorted by their emission line classification. The cut outs are $40 \times 40\,h^{-1}$ kpc in size.

on the [N II] diagram, we define a new empirical Seyfert–LINER separation:

$$\log([O\,III]/H\beta) = 1.05\log([N\,II]/H\alpha) + 0.45. \qquad (1)$$

2.5.2 Classification results

Following the emission-line classification we divide our early-type galaxy sample into five classes:

(i) quiescent (orange);
(ii) star forming (blue);
(iii) transition region (purple);
(iv) Seyfert (green);
(v) LINER (red).

Most objects in the quiescent early-type galaxy class are virtually free of emission lines. A small subfraction exhibits weak [O III] emission, but lack the other emission lines necessary for the BPT classification. We verified that a further separation of this subclass does not affect the results of this work. The quiescent objects make up the bulk of the early-type population (82 per cent). The early-type galaxies with significant emission lines (S/N > 3 in the four main BPT lines) represent the remaining fifth of the early-type sample. We call these active early-type galaxies, and separate them into star forming, transition objects, Seyferts and LINERs. The results of this classification are summarized in Table 1. For further details we refer the reader to the paper describing the MOSES catalogue (Schawinski et al., in preparation). We show some example images of morphological early-type galaxies in Fig. 3.

Table 1. Emission line classification results.

Classification	Number	Fraction galaxies	Colour
Early-type galaxies	15 729	100 per cent	
Quiescent	12 828	81.5 per cent	Orange
Star forming	671	4.3 per cent	Blue
Transition region	1 087	6.9 per cent	Purple
Seyfert	242	1.5 per cent	Green
LINER	901	5.7 per cent	Red

2.5.3 Star formation rates

For those galaxies classified as star forming, we derive SF rates from the extinction-corrected Hα line luminosity according to the conversion of Kennicutt (1998). All SF rates for our galaxies quoted in this paper are based on Hα unless otherwise noted. We cannot derive reliable SF rates for any of the other emission line classes, as an unknown fraction of the Hα emission line is of non-stellar origin.

3 STELLAR POPULATION ANALYSIS

The spectrum of a galaxy contains a record of its SF history over the age of the universe. Its stellar populations are the combination of all the episodes of SF that a galaxy and its progenitors underwent. Reconstructing this SF history or at least recovering it partially is a challenging task that requires excellent observational data, stellar population models for the interpretation and a statistically sound method for the recovery.

For the problem at hand in this paper, we turn to the parametric approach. It has been used with great success by Ferreras & Silk (2000) and by Kaviraj et al. (2007) to use the immense discriminating power of rest-frame NUV and FUV photometry to test whether individual early-type galaxies have undergone episodes of recent residual SF or not.

3.1 Two-component star formation histories

The aim of this work is the mapping of current SF/AGN activities in galaxies with their SF histories. Of particular relevance for us is the epoch and the strength (hence mass fraction) of the last significant starburst that occurred in a galaxy. Since the most recent episode of SF dominates the spectrum at all wavelengths, it is the easiest to recover (see Fig. 4). Following the approach of Kaviraj et al. (2007), we therefore fit two-component SF histories to the galaxy data.

The old component is modelled as an instantaneous starburst of variable age and metallicity, and represents the formation of the bulk stellar population of the galaxy before the most recent episode of SF. We allow this old component to vary between a t_o of 1 and 15 Gyr. By marginalizing over this parameter later on, we are summing all possible linear combinations of single starbursts and so take into account all possible SF histories before the most recent starburst.
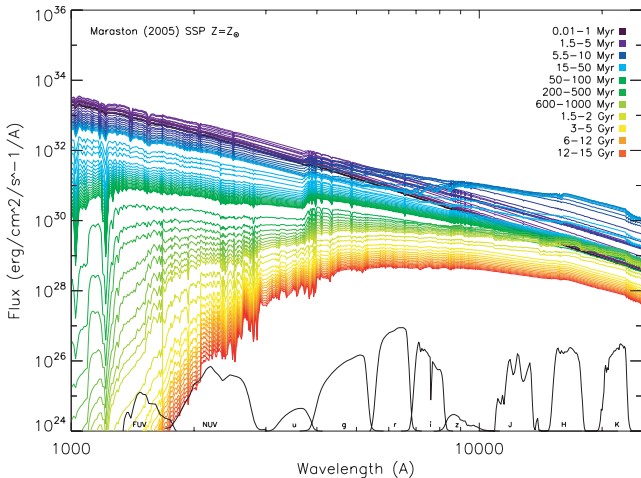
Figure 4. The pace of stellar evolution: we show the SED of a solar metallicity M05 SSP from 0.01 Myr to 15 Gyr. The different ages are colour coded and we indicate the filters we use by their filter transmission curves of the data we use in this paper at the bottom. The broad-band colours of a galaxy will always be dominated by the youngest stellar population formed in the most recent episode of SF. Any older population will be small by comparison even with respect to a relatively small young mass fraction. This feature of stellar evolution allows us to effectively split the SF history into two components until about 1.5–2 Gyr when the pace of stellar evolution slows down and populations of different ages up to 15 Gyr become similar and the differences are on the order of the effects of dust and metallicity.

On top of this, we add a young component of a certain age t_y and mass fraction f_y. It turns out that this young burst is poorly modelled by an instantaneous starburst, so that we choose to represent it by an exponentially declining SF rate with an e-folding time of 100 Myr. The choice of 100 Myr is motivated by a test on a small subsample, where we left the e-folding time τ as an additional free parameter. In this test, we recovered a typical τ of ~100 Myr for early-type galaxies with young components, so we set τ to 100 Myr a posteriori. The parameter t_y stands for the look-back time to the beginning of the starburst, f_y is the total mass fraction formed in the recent burst extrapolating the 100 Myr e-folding SF history to infinity. Since virtually all ages we recover for the starburst population are at least ~100 Myr, the difference between the mass actually formed by today and the total mass that will form is small.

This parametric quantification of the age and mass fraction of the secondary population allows us to derive a recent SF history against the background of any possible SF histories in the distant past, represented by a simple stellar population (SSP), whose effect we can account for by marginalization. This approach is different from purely non-parametric approaches in the literature that make no a priori assumptions on the SF history to be recovered (e.g. Panter, Heavens & Jimenez 2003; Panter et al. 2007).

3.2 Internal metallicity distribution

Besides assigning an average metallicity to each model, we additionally consider the internal distribution of metallicities necessarily present in each galaxy. This is important, as a tail of low metallicity stars can have a significant effect in particular on the ultraviolet part of the spectrum (Maraston & Thomas 2000). We construct an analytic form of the typical metallicity distribution from observations of the bulge of M31 and the closest early-type galaxy NGC 5128 where individual stars can be resolved (Harris, Harris & Poole 1999;

Harris & Harris 2000, 2002; Sarajedini & Jablonka 2005). This metallicity distribution is modelled with two Gaussians. The bulk metallicity is a Gaussian with a mean metallicity μ_Z and a spread of $\sigma = 0.22$ dex, while the tail is parametrized as a Gaussian shifted by 0.75 dex to lower metallicity with the much larger spread of $\sigma = 1.5$ dex. Both components are such metallicity composites, and we vary μ_Z to cover a mean mass-weighted metallicity $Z(\mu_Z)$ ranging between ~1/200 and ~3.5 $Z_\odot$.

3.3 Dust extinction

Internal dust extinction causes a degeneracy with age and mass that needs to be taken into account. To describe dust attenuation we adopt the extinction law by Calzetti et al. (2000). This choice is mainly motivated by the fact that the active early-type galaxies in our sample are undergoing significant episodes of SF, so that an extinction law derived from a sample of star-forming galaxies seems reasonable. In separate runs we have tested a number of other extinction laws (Milky Way Allen 1976; LMC Fitzpatrick 1986; SMC Prevot et al. 1984; Bouchet et al. 1985) and verified that in general, the Calzetti et al. (2000) law provides the best fits. The dust parameter $E(B - V)$ is varied between 0.0 and 0.8.

3.4 Combining photometry and spectroscopy

A crucial novelty of our approach is the combination of photometric and spectroscopic data, which increases the power of breaking the degeneracies between age, mass, metallicity and dust content. The reason why this helps is that the degeneracies are different because of the dissimilar non-linear responses of broad-band colours and stellar absorption indices to these parameters. Like cosmologists who combine the very degenerate contours of one experiment with another to find a well-constrained set of parameters in the intersection, we harness two very different observables that couple to the fundamental physical parameters in very different fashions.

It should be noted that absorption line indices are not significantly affected by dust (MacArthur 2005). A further cornerstone in our fitting algorithm for the identification of intermediate-age populations is the inclusion of near-infrared (IR) photometry and stellar population models (Maraston 2005) that adequately describe the thermally pulsing asymptotic giant branch (TP-AGB) phase. This is crucial as the TP-AGB provides most of the near-IR light of a stellar population between 0.5 and 2 Gyr (Maraston 1998).

In a nutshell, we perform a comparison of the observed photometric spectral energy distribution (SED) (of as many as are available of FUV, NUV, *u, g, r, i, z, J, H, K*) to a library of SEDs of over five million two-component SF histories from Maraston (2005) and compute the appropriate model SED parametrized by the five parameters described above (t_y, f_y, t_o, μ_z and $E(B - V)$) compute the associated χ^2 statistic to obtain a probability distribution function for those five parameters. An intrinsic error for our photometry across all filters of 0.015 mag is adopted to deal with the uncertainties in the absolute photometric calibration of SDSS.

Simultaneously, we compute the associated luminosity-weighted SSP ages and metallicities for each model. We derive luminosity-weighted SSP ages and metallicities by χ^2 fitting the Thomas, Maraston & Bender (2003) and Thomas, Maraston & Korn (2004) models to the 25 Lick absorption line indices and compute a second probability distribution through the comparison of these quantities with the *V*–luminosity weighted ages and metallicities of the photometric comparison. These two probability distributions from the SED and absorption-line fitting are then convolved to the final one.

In order to estimate the parameters of interest, we marginalize the resulting five-dimensional probability distribution function to obtain the two-dimensional distribution in the recent starburst age versus mass-fraction plane (t_y–f_y). We integrate over this surface to obtain confidence levels constraining the age and mass-fraction of the last significant episode of SF in the galaxy. These probability distributions are stacked to get typical values for the subpopulations.

3.5 Example galaxies

In this section we present two example fits to galaxies with very different properties and SF histories. The first galaxy is an active early type in the transition region of the emission-line classification which suggests that the object is dominated both by ongoing SF and an AGN. Its Hα SF rate is 2.1 M$_\odot$ yr^{-1} and its UV-optical colours place it squarely into the blue cloud ($u - r = 2.3$, NUV $- r = 3.2$). The second galaxy is a typical passive quiescent early-type galaxy with no detected emission lines. Its UV-optical colours place it on the red sequence ($u - r = 2.8$, NUV $- r = 6.1$). The availability of GALEX, NUV and FUV photometry generally improves the confidence contours, but does not shift the best fit.

The fit results are summarized in Figs 5 and 6. In panel (a) we show the fit to the photometry: in black are the observed broad-band colours with the errors magnified by a factor of 3 to make them visible. To guide the eye, we show the filter transmission curves of the various filters used from GALEX far-UV to 2MASS K band. The best-fitting model is shown in green and the separate old and young components are red and blue, respectively. We also show the SDSS colour images.

In panels (b) and (c) we show the probability distributions for the luminosity-weighted age and metallicity derived from the absorption-line indices. The final result in the t_y–f_y plane is shown

in panel (d). This plot quantifies strength and epoch of most recent episode of SF. In panels (e) and (f), we show the projected, projected probability distributions for the parameters t_y and f_y. In the main analysis we will stack these distributions for various classes of galaxies. In panels (g) and (h), we show dust extinction $E(B - V)$ and the age of the old component.

The two example galaxies show very different SF histories. The active galaxy has a very young luminosity-weighted age, which is well consistent with the increased UV flux. The two-component SED fit yields an old component of 3 Gyr and places the most recent starburst at an age of 400 Myr with a mass fraction of 7 per cent. Its dust content is relatively high ($E(B - V) = 0.1$) in agreement with the current SF activity. The low luminosity-weighted age of the 'old' component implies that this object had several rejuvenation events in the past.

The emission line free galaxy, instead, has an old luminosity-weighted age derived from the spectroscopic data. The two-component fit yields basically two old components with ages around 10 Gyr. We can conclude that this galaxy clearly has not undergone a significant starburst in the recent past, while the details of its SF history in the more distant past are not resolved. The 99 per cent confidence intervals exclude any sort of significant SF activity in the recent past. The very low dust attenuation value fits well into this picture.

We also note that while only a fraction of the galaxies in our sample have GALEX, their fitted SF histories do not differ significantly from those without.

4 RED SEQUENCE AND BLUE CLOUD

In this section, we discuss the position of the various galaxy classes defined through the emission-line diagnostics in the colour–mass relation. This simple comparison allows us to draw first tentative
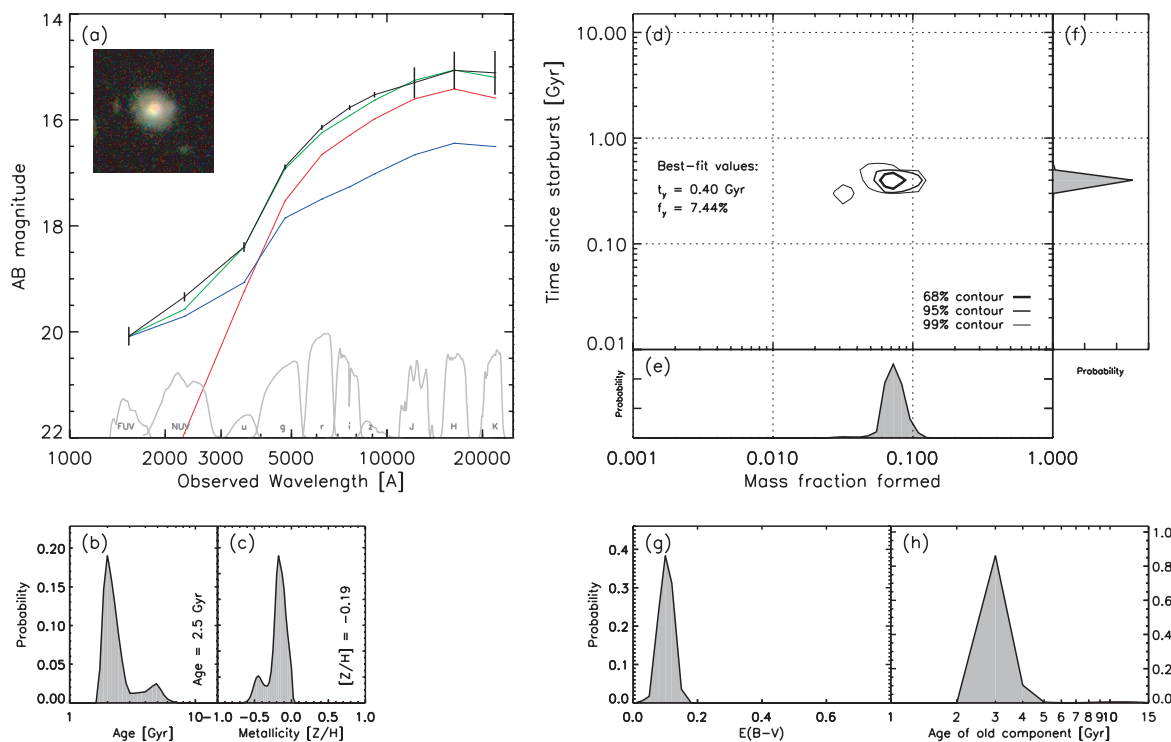

Figure 5. An example of a galaxy where we can resolve and quantify the last significant episode of SF. This object is a star-forming early-type galaxy. For a detailed description, see Section 3.5.
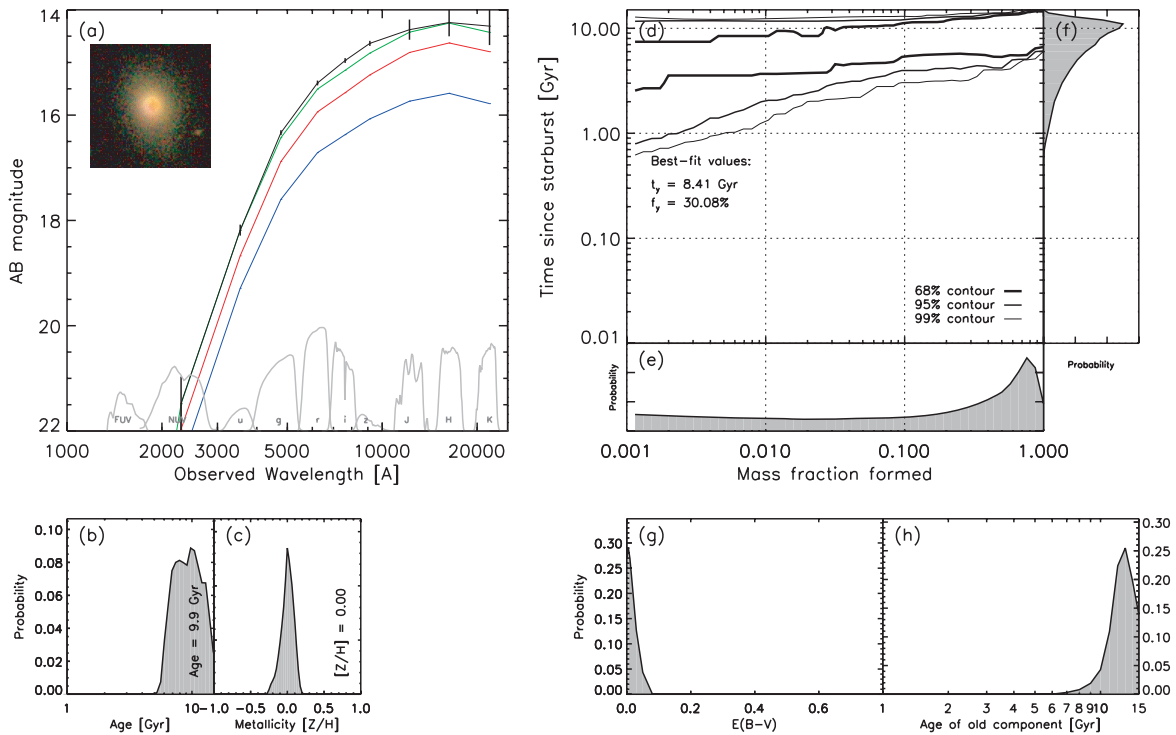
Figure 6. An example of a galaxy where we cannot quantify the first significant episode of SF, but can place strong limits on the recent SF history. For a detailed description, see Section 3.5.

conclusions that are independent of our stellar population analysis method. Quantitative results of the detailed analysis will be presented in the subsequent section.

4.1 Active galaxies in the colour–mass relationship

In Fig. 7 we show $u - r$ colour as a function of galaxy velocity dispersion σ for the galaxies in our sample. The morphological late-type galaxies are shown as grey points, the early-type galaxies are coloured points subdivided in the various emission-line classes: quiescent (i.e. no emission lines, orange), LINER (red), Seyfert (green), transition (purple) and star forming (blue). The quiescent early-type galaxies (see most right-hand panel) form the well-known red sequence, while the late-type galaxies in the sample define the so-called blue cloud (grey points).

The first key result of this work is that the active galaxies are offset from the red sequence and exhibit well-defined patterns across the colour–σ diagram. Star-forming objects inhabit the blue cloud. While this may seem like an obvious result, note that the broad-band SED and the emission lines probe very different physical components of a galaxy. While the former traces the stellar populations and therefore the past, fossil record, the emission lines provide information on the current state of the ionized gas in the galaxy. It is very reassuring that objects with ongoing SF show significant rejuvenation also in their stellar populations.

More importantly, those objects not dominated by SF but by AGN activity, Seyferts and LINERS, are located considerably closer to and almost on the red sequence. Transition objects, instead, which are composites of SF and AGN activity are found right between these two extremes. There is a sequence between the blue cloud and the red sequence from star forming via transition region and AGN to quiescence. In more general terms, the presence of AGN

in a green valley between the blue cloud and the red sequence has been discussed in other recent work in the literature (Faber et al. 2007; Graves et al. 2007; Kauffmann et al. 2007; Martin et al. 2007; Nandra et al. 2007; Salim et al. 2007; Wild et al. 2007).

4.2 Mass dependence

This tentative sequence is convolved with a clear mass dependence of the emission-line classification. The blue star-forming objects are found at the low-mass end, while the majority of early-type galaxies classified as LINERs lie at the high-mass end on the red sequence. Transition objects and Seyferts reside between these two extremes also in their galaxy mass distributions.

The presence of a significant fraction of low-mass early-type galaxies showing signs of ongoing SF of a few $M_{\odot}$ per year (see Fig. 8) is a striking result, which is mostly the merit of the pure morphological selection strategy. Still, this result is not surprising. The GALEX UV satellite has found evidence for minor recent SF in early-type galaxies (Yi et al. 2005), and the SAURON (Spectrographic Areal Unit for Research on Optical Nebulae) survey of 48 nearby elliptical and lenticular galaxies has shown that many of them have (often extended) emission lines and signs of recent SF as well as CO emissions from molecular gas and atomic hydrogen indicating sometimes substantial reservoirs of gas (Morganti et al. 2006; Sarzi et al. 2006; Combes, Young & Bureau 2007).

In general, low-mass early-type galaxies are well known to show young stellar ages, emission lines and even ongoing SF. This downsizing of galaxy formation, wherein the most massive galaxies harbour the oldest stellar populations is now generally accepted. Today's early-type galaxies in particular show a clear correlation between mass and age (Caldwell, Rose & Concannon 2003; Nelan
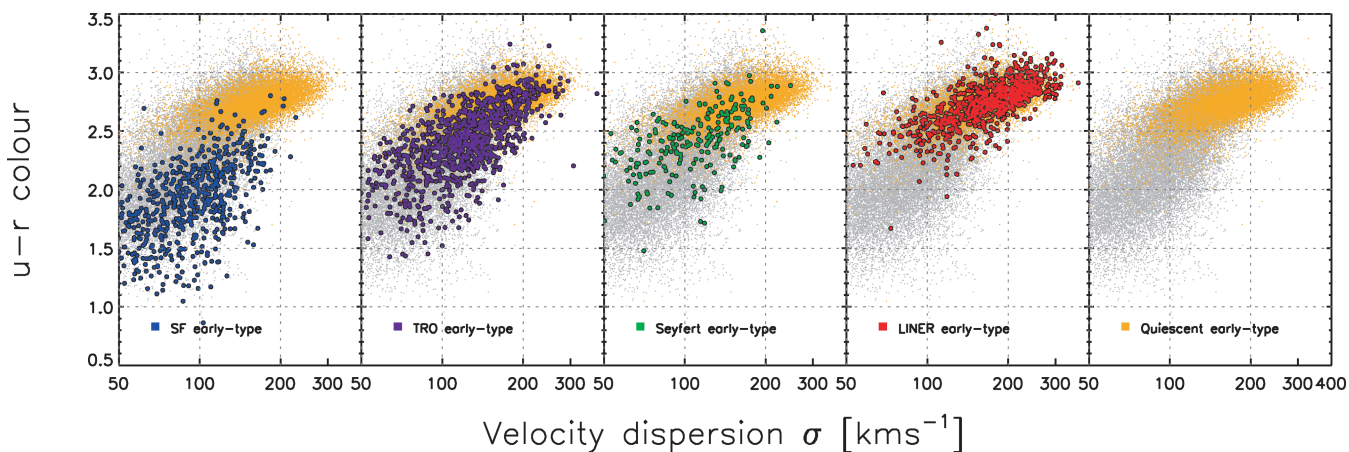
Figure 7. The colour–σ relation for our sample. In each panel, morphological late-types are grey, quiescent early-types are orange and the various active early-types are blue (star forming), purple (transition region), green (Seyfert) and red (LINER). The mass tracer is the stellar velocity dispersion.

et al. 2005; Thomas et al. 2005; Bernardi et al. 2006; Jimenez et al. 2006).

Fig. 7 shows that our sample comprises a large, statistical subsample of active early-type galaxies in the intermediate-mass and low-mass regimes ($\sigma \lesssim 200 \, \mathrm{km \, s^{-1}}$) allowing us to study the interplay between SF, nuclear activity and quiescence in early-type galaxies. We note that many of the high-mass transition region objects are most likely misclassified LINERs. They do not have any star forming or Seyfert counterparts at the same mass.

4.3 AGN feedback in action?

At low and intermediate masses we can identify a sequence at a given mass from SF via transition region and AGN activity to quiescence, which is echoed in a sequence from blue to red stellar populations. Taking $u - r$ colour as a proxy for the stellar age and hence using the stars as cosmic clock, this is highly suggestive of an evolutionary sequence. We are observing the act of galaxy transformation from the star forming blue cloud via the green valley to the passive red sequence in action.

We interpret the deviation from the red sequence as rejuvenation due to a recent episode of SF. On their way back to the red sequence, galaxies appear to pass through a phase of significant nuclear activity, as transition region objects and Seyferts have colours between

Figure 8. Histogram of the SF rate and specific SF rate of the star-forming early-type galaxies. The SF rate is based on the luminosity of the Hα line and is converted to a rate using the relation of Kennicutt (1998).

the blue star forming and the red sequence objects. This indicates that AGN may have a decisive role to play in this transformation process. Fig. 7 suggests that residual SF and nuclear activity are connected in early-type galaxies. It is possible that the AGN actually suppress the SF activity, and we are witnessing AGN feedback in action. Our sample represents the ideal laboratory to probe these processes.

It should be noticed that the massive early-type galaxies in our sample do not appear to be part of such transformation process. At the high-mass end only quiescent and LINER objects are found.

What needs to be shown is twofold. First, solid evidence for the presence of an evolutionary sequence for the low/intermediate-mass objects is required. To this end, we have derived detailed SF histories using the method presented in Section 3 focusing on the epochs and mass fractions of the most recent starburst. This allows us to investigate whether the galaxies of the various subclasses in our sample truly belong to the same object type at different evolutionary stages. Second, the interaction between SF and nuclear activity along this sequence must be investigated, with the aim to understand whether and how the two processes are related. These are addressed in the following sections.

5 THE EVOLUTIONARY SEQUENCE

Following the discussion of the previous section we divide our sample in three velocity dispersion bins ($\sigma \leqslant 100 \, \mathrm{km \, s^{-1}}$, $100 < \sigma \leqslant 200 \, \mathrm{km \, s^{-1}}$, $\sigma > 200 \, \mathrm{km \, s^{-1}}$) representing low-mass, intermediate-mass and massive early-type galaxies. Within each σ bin we maintain the five subclasses: star forming, transition object, Seyfert, LINER and quiescent. Within each of the 15 resulting subclasses we stack the probability distributions for the SF histories obtained in the analysis of Section 3. We marginalize over all parameters except the mass fraction f_y and age t_y of the starburst component. The resulting contours of the probability distributions in the t_y–f_y plane are shown in Fig. 9. The panels are analogues to panel (d) of Figs 5 and 6. The five columns show the various emission-line classes, the rows are the three σ bins. A bar in each panel indicates the relative fraction of objects in this particular subclass.

5.1 Evidence for the time sequence

The results shown in Fig. 9 allow one immediate conclusion. The SF histories derived for the low-mass and intermediate-mass objects
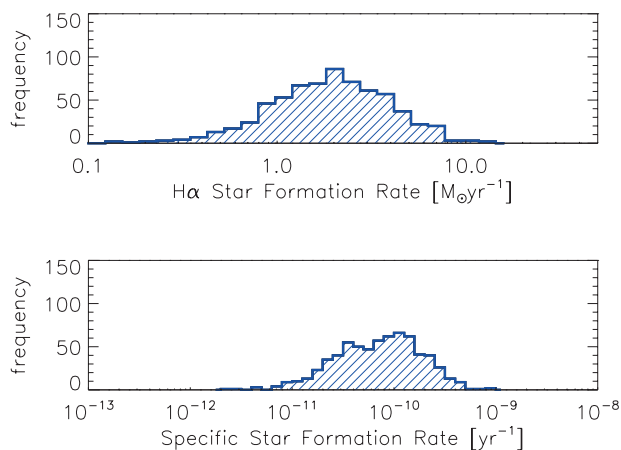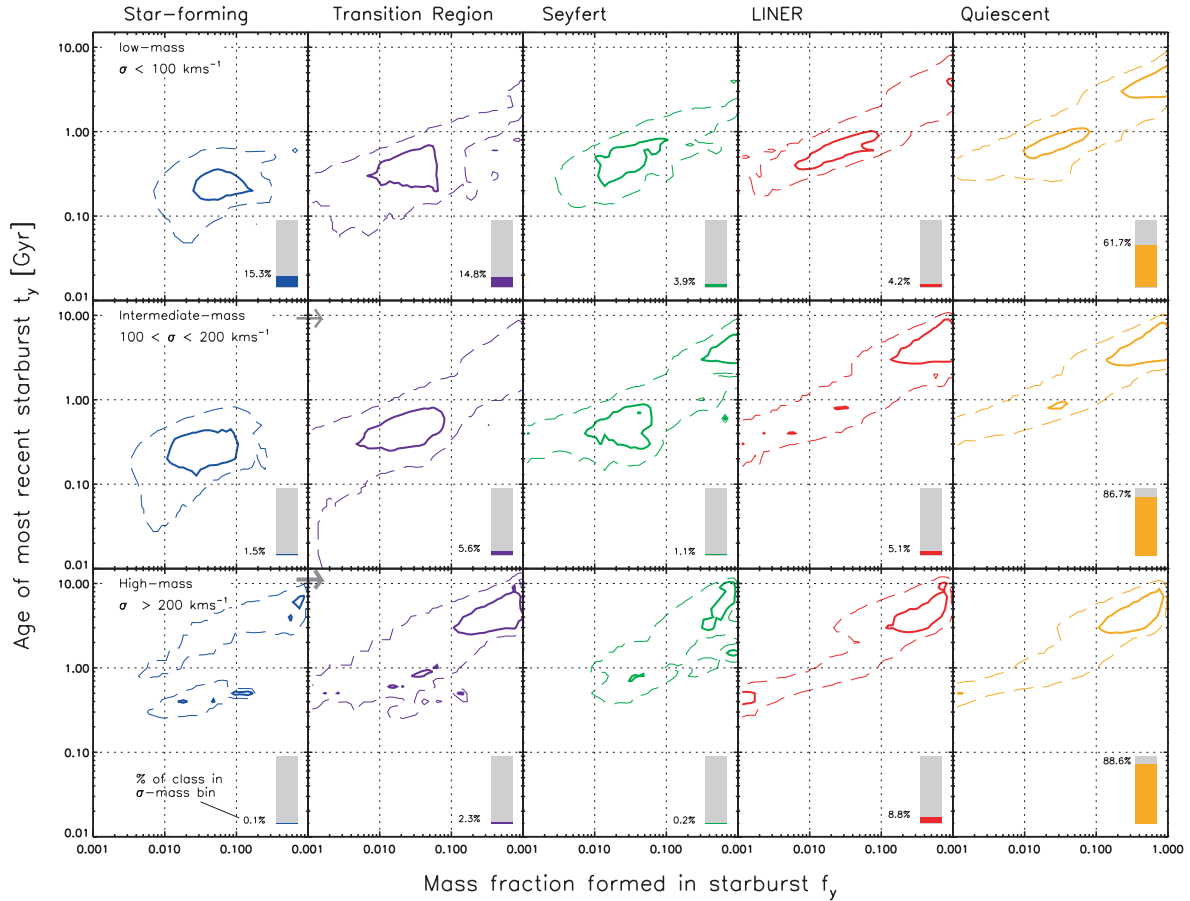
Figure 9. The recent SF histories of early-type galaxies by mass and emission line class. In the horizontal direction, we split our sample into three velocity dispersion bins. Vertically, we split the galaxies in each σ bin by their activity type from star forming to quiescent (cf. Fig. 7). The contours are 25 and 50 per cent probability contours, respectively. Note that the area of these contours can be misleading; only a small fraction of early-type galaxies is in classes other than the quiescent bin. In order to guide the eye, we indicate the fraction of galaxies in each mass bin (low, intermediate and high) that are in each emission line class. For example, in the high-mass regime, only a tiny fraction of early-types are classified as star forming (most likely misclassifications), while the almost 90 per cent are quiescent; nevertheless, the contours occupy similar areas on the t_y–f_y plane.

in our sample galaxies reveal clear evidence for the occurrence of a starburst between 100 Myr and 1 Gyr in the past involving a typical mass fraction of 1 to 10 per cent. This reinforces the interpretation of deviations from the red sequence in the colour–σ diagram (see Fig. 7) to be caused by recent rejuvenation events. Key is the epochs and mass fractions of this rejuvenation for the various emission-line classes. While the starburst ages clearly increase from star forming via AGN dominated to quiescent in a continuous sequence from ~100 Myr to beyond 1 Gyr, the mass fractions remain the same. This points to the various emission line classes having undergone the equivalent rejuvenation event in the past, and the only feature differentiating the various classes is the time elapsed since that SF episode. Hence, the objects of the various emission classes in the panels along one row in Fig. 9 are identical in terms of mass, morphology and SF history, except that the epoch of the last starburst varies. This means we have resolved an evolutionary sequence, and what we are seeing is the process of rejuvenation in early-type galaxies at different evolutionary stages. This time sequence includes a phase of AGN activity along the way.

The fraction of objects taking part in this transformation is strongly dependent on mass. In the lowest mass bin about one third of the objects shows emission lines and is caught in the process of this transformation. This fraction drops to 13 per cent in the interme-

diate mass bin containing galaxies with $100 \leqslant \sigma < 200\,\mathrm{km\,s^{-1}}$. In the highest bin for objects with velocity dispersion above $200\,\mathrm{km\,s^{-1}}$ the evolutionary sequence is not detected. At the high-mass end, the vast majority of galaxies is quiescent, and no recent starburst within the past few Gyrs has occurred. The small fraction of active galaxies is by far dominated by LINER-like emission, with some transition region objects that are in fact closer to the properties of LINERs (see Section 6.5.3).

5.2 Time-scales along the sequence

For the low- and intermediate-mass objects ($\sigma < 200\,\mathrm{km\,s^{-1}}$) we can now determine the relative and absolute timing of this transformation process. We marginalize over the mass fraction and compute the stacked probability distributions of starburst ages for the various emission-line classes. The result is shown in Fig. 10 for the low- and intermediate-mass early-type galaxies in the left- and right-hand panels, while in Table 2, we give the figures in Myrs. In both mass bins, we can see the shift in the age of the last episode of SF in a sequence as could already be seen from Fig. 9. The star-forming objects are clearly the ones most recently rejuvenated with starburst ages around 150–300 Myr, with the latter increasing along
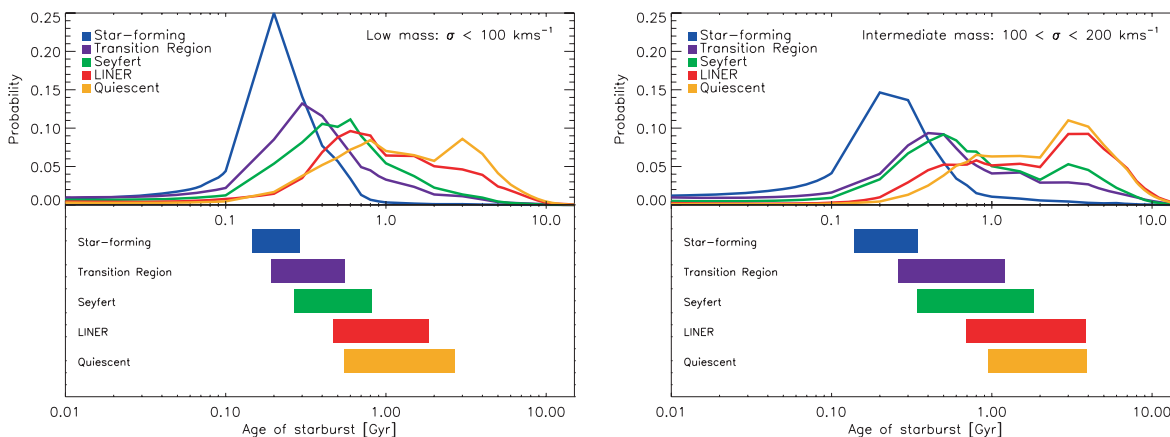
Figure 10. The time sequence in the low- and intermediate-mass bin: in the top of each panel, we show the stacked, normalized probability distribution functions for the time elapsed since the start of the starburst t_y. In the bottom, we indicate where on the t_y axis 50 per cent of the probability lie. We give the numbers for this in Table 2.

Table 2. The time sequence: the age of the last episode of SF as a function of mass and emission line class.

Mass regime	Velocity dispersion (km s^{-1})	Star formation (Myr)	Transition region (Myr)	Seyfert AGN (Myr)	LINERs (Myr)	Quiescent (Myr)
Low mass	0–100	145–280	195–550	270–800	470–1800	550–2700
Intermediate mass	100–200	140–350	260–1200	350–1800	700–4000	950–4000

Note. The time intervals given in this table correspond to the 50 per cent probability intervals from Fig. 10.

the sequence from transition region through Seyfert and LINER to quiescent.

A global interpretation yields the following picture: the most common starburst age t_y for the transition region objects is around 300 to 500 Myr. Seyfert activity appears further 100 to 300 Myr later with starburst ages peaking at about 600 Myr. This phase is followed by LINER and quiescent with separations of a few 100 Myr, respectively. The widths of the distributions increase along this sequence from about 200 Myr for the star-forming objects to 400–600 Myr in the transition region and Seyfert objects. The phases involving nuclear activity, transition and Seyfert, appear to be of comparable length in time and must be a factor of 2 to 3 longer than the star forming one. Note that the widths of LINERs and quiescent objects are much less well determined as they extend into the regime of old ages beyond 1 Gyr, in which the age resolution is significantly reduced.

The transition region and the Seyfert phases seem to overlap considerably, which suggests that objects at this point along the time sequence may switch back and forth between transition region (a mixture of AGN and SF) and Seyfert phase (pure AGN). If this is the case, the Seyfert phase represents episodes of enhanced accretion on to the black hole between phases with lower levels of nuclear activity together with low residual SF. The SF we see in the transition region objects may even be induced by the (potentially) recurrent Seyfert state as the jets and outflows pile up gas before finally pushing it out (Silk & Rees 1998; Silk 2005).

Toward the end of the sequence, the transition from the high-ionization Seyfert phase to quiescence passes through a phase of nuclear activity characterized by low ionization (LINER). In total, the transformation process from blue cloud to red sequence passing through nuclear activity takes about 800 Myr to 1 Gyr.

5.3 Lifetimes and number fractions

An important consistency check is the comparison of the lengths of the various phases as derived from the stellar population ages with the number of objects found in each phase. If the transition region and Seyfert phases are equally long, the number of objects found in these two classes must be the same. From Fig. 9 it can be seen that this is not the case. We observe three to four times more transition region objects than Seyferts. However, an unknown fraction of the objects in the Seyfert phase must be Seyfert type I rather than type II depending on the viewing angle from which the nucleus is seen. Indeed, broad emission line objects like type I Seyferts are not classified as 'galaxies' by the SDSS spectroscopic pipeline and hence are not included in our sample. Thus, it is plausible that the ostensible lack of Seyfert AGN in our sample stems from this geometric effect, which puts object numbers and phase lifetimes in very good agreement. It should also be noted that our sample is not volume limited.

5.4 Dependence on mass

The comparison between the lifetimes of the star forming and AGN phases is more complex, as an additional mass dependence comes into play. The fractions of the active early-type galaxy population in a given mass bin that are classified as transition region and Seyfert objects decrease by about a factor of 2.5 from the low- to the intermediate-mass bin, while the number of star-forming objects decreases by a factor of 7. This results in a factor of 3.5 more transition region objects than star forming ones at intermediate masses, while their fractions are comparable at low masses. As the transition region phase lasts about two to three times longer than the

star forming one in both mass regimes this suggests that not all low-mass objects go through the time sequence. Hence SF is not followed by nuclear activity in all cases, and the true proportions between star forming and transition region objects for the SF–AGN sequence may be observed only at intermediate mass. This implies the presence of a tail of young quiescent objects in the low-mass bin, which is indeed indicated by the probability distributions in Fig. 10.

Still, the ratio transition region to star-forming objects seems slightly too high at intermediate masses. The reason for this may be that some fraction of transition objects are misclassified and are actually LINERs (see Section 6.5.3). This would also explain why transition objects and Seyfert appear less well separated at intermediate mass.

Within these uncertainties, the fraction of galaxies that experiences residual SF, and transitions from starburst to quiescence via nuclear activity drops by about a factor of 2 to 4 between the low-mass and the intermediate-mass bins. The highest mass bin ($\sigma > 200 \, \mathrm{km \, s^{-1}}$) concludes this trend, as no such sequence is detected for these masses. This is very well supported by the fact that the apparent dichotomy in the starburst age distribution within the quiescent early-types galaxies (left-hand panel of Fig. 10) is considerably weaker at intermediate masses (right-hand panel), and disappears entirely at the high-mass end (see Fig. 9).

Finally, it is interesting to note that, while the vast majority of LINERs detected in the low-mass bin appears to take part in the evolutionary sequence, the presence of a second independent LINER population seems to emerge at intermediate masses. Fig. 10 reveals a clear dichotomy with a fair fraction of LINER-like objects that does not show signs of recent rejuvenation. This trend becomes even more evident at the highest masses, where the largest fraction of LINERs is detected (8 per cent), which contain only old stellar populations (see Fig. 9).

5.5 Dust properties along the sequence

Fig. 11 shows the stacked, normalized probability distribution functions for the dust parameter $E(B - V)$ obtained through our SED fitting algorithm for the low- and intermediate-mass bins. The different line styles are the various emission-line classes (see labels).
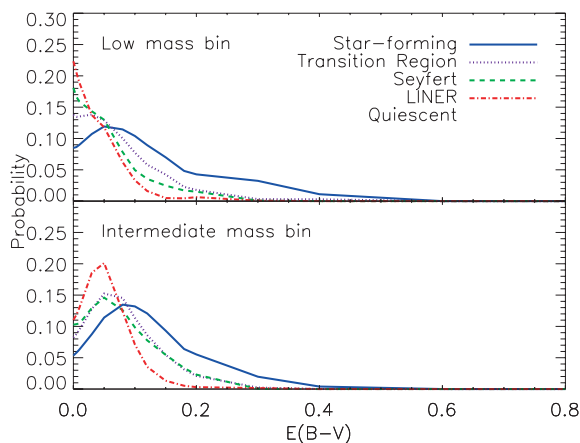

Figure 11. This plot shows the stacked, normalized probability distribution functions for the dust parameter $E(B - V)$ for the low- and medium-mass bin. Star-forming early-types are the dustiest with the transition region, Seyfert early-types being less dusty and the LINERs and quiescent early-types containing even less dust.

As ought to be expected, dust content decreases along the sequence discussed above with highest dust attenuation in the star-forming objects ($E(B - V) \sim 0.1$) and the lowest in the quiescent ones ($E(B - V) \lesssim 0.05$). This internal consistency further strengthens the conclusion that we are indeed observing a time sequence and are witnessing the transformation of early-type galaxies from SF via AGN to quiescence. In order to mimic a time sequence in the observed $u - r$ colours with a variation in the amount of dust rather than in age, the trend in $E(B - V)$ would have to be the opposite of what we observe.

6 DISCUSSION

With Fig. 7 in Section 4 we show that early-type galaxies of different emission-line classes occupy different loci in the colour–σ diagram. Star forming early types are the bluest deviating most from the red sequence. Once some AGN contribution appears in the optical emission lines, the colours dramatically redden. In Section 5, we demonstrate quantitatively that there is indeed strong evidence for the existence of an evolutionary sequence of early-type galaxies moving from the blue cloud to the red sequence (Salim et al. 2007). We show that on this path the galaxies go through a number of phases starting at SF followed by a transition region of SF and AGN, a Seyfert AGN phase and a LINER phase before finally settling to total quiescence and passive evolution on the red sequence. This process is currently building the low-mass end of the red sequence in the low redshift universe. In this section we discuss the astrophysical implications of this finding, the role of LINER-like early-type galaxies, possible trigger mechanisms of this sequence and follow-up observational campaigns in the context of the time sequence we have derived.

6.1 The starburst–AGN sequence

A clear implication of our results is the existence of a link between residual starburst and nuclear activity at recent epochs in low- and intermediate-mass early-type galaxies. Whatever triggers the starburst, it leads also to an AGN, and the star-forming phase reaches quiescence via an AGN phase. We see the starburst fading while the AGN rises. This leads to two possible scenarios depending on whether the two processes, SF and AGN, are connected.

6.1.1 AGN feedback or black hole growth in action?

If the fading of SF and nuclear activity are linked, then we are observing AGN feedback in action. The appearance of the AGN in the transition region and Seyfert phases are concurrent with the end of SF, so it is plausible that these two phenomena are connected such that the rise of the AGN suppresses and terminates SF by heating and expulsion of the remaining gas.

Alternatively, it is possible that starburst and AGN actually do not interact with each other, even though they may be triggered by the same global event. In this case SF fades simply owing to supernova feedback and/or the exhaustion of cold gas. Most interesting in the framework of this scenario is our finding that the AGN rises while SF declines. This shows that in this case AGN activity must be delayed substantially with respect to the starburst by several hundred Myr and may actually be triggered by SF. This delay might be the result of slow AGB winds fuelling the black hole (Davies et al. 2007). This implies that the early-type galaxy or its progenitor hosting the starburst is just in the process of building up its central supermassive black hole.

6.1.2 Gas depletion time-scale: in favour of AGN feedback

In order to distinguish these two scenarios, we compare the observed time-scale for the fading of SF with simple theoretical estimates based on the Schmidt–Kennicutt law (Schmidt 1959; Kennicutt 1998). The latter relates the SF rate with the ratio of gas mass surface density and the dynamical time-scale of the system scaled by an efficiency ϵ. We assume that the dynamical time-scale of SF is on typical galaxy time-scales of $\sim$0.1–0.5 Gyr, as observed in gas discs in elliptical galaxies (Young 2002). We can exclude shorter dynamical time-scales caused by a concentration of the starburst activity to small radii, as the mean petrosian half-light radii of the u-band light in the star-forming early-types (2.25 arcsec) imply that SF in these objects is extended over several kpc. Then to deplete any gas reservoir would take on the order of many Gyr.

This time-scale is significantly longer than the fading time-scale deduced here for our sample galaxies. In our modelling analysis we find that the recent rejuvenation event is best modelled by a exponentially declining starburst with e-folding time-scale around 100 Myr. Thus, the gas reservoir cannot get depleted solely via self-regulated SF. An additional heating source is required. The fact that we find an AGN phase subsequent to the starburst strongly suggests that the AGN is (at least partly) responsible for the suppression of SF by depleting the gas reservoir accelerating the transition from the blue cloud to the red sequence. A more detailed investigation of this process is beyond the scope of this paper. It will be explored in more detail in a forthcoming work (Kaviraj et al., in preparation).

This argument strongly supports the AGN feedback interpretation of the time sequence. This result has important consequences for our understanding of galaxy formation. It is empirical proof that AGN feedback, the existence of which is now postulated in most recent models of hierarchical galaxy formation (see Introduction and references therein), occurs in early-type galaxies at late stages of their evolution. Beyond this important conclusion, our sample that is resolving the actual sequence of AGN feedback provides further insight into this process. We find its overall time-scale to be of the order of a Gyr. Moreover, we observe a substantial delay between fading of SF and rise of the AGN by a few hundred Myr, which might reflect the time-scale required for the black hole to build up the accretion disc. This implies that AGN feedback is not well approximated with an immediate truncation as implicitly assumed in current hydrodynamical simulations (Springel et al. 2005a).

6.2 Obscured AGN?

A key result is that we see the AGN rising while SF fades. As absolute O[III] luminosities increase along the sequence, it can be excluded that the AGN is simply out-shined by the starburst during the star-forming phase. However, it is still possible that the AGN is not observed during the starburst, because it is highly obscured in the beginning. In this case, SF and AGN would co-exist from the beginning, and while SF fades, the AGN remains active. This does not invalidate but rather strengthen the interpretation of AGN feedback occurring in our sample galaxies.

6.3 Progenitors and trigger mechanisms

The youngest early-type galaxies on the evolutionary sequence we resolve are the star forming ones with starburst ages around 100–200 Myr. The progenitors of these objects within the sequence must have stellar populations younger than 200 Myr. The fact that we do not observe these objects implies that they are excluded through our selection criteria, hence they most likely do not have early-type morphology.

6.3.1 Prodigious star formation in the recent past

As we model the starburst as composite stellar population with exponentially declining SF histories, these progenitors must have had significantly higher SF rates in the past. The typical star-forming early-type galaxy has a mass of about 5×10^{10} M$_\odot$ and has formed about 5 per cent of its stellar mass in the current burst (i.e. 2.5×10^9 M$_\odot$) over the last 100 Myr. This corresponds to an average SF rate of 25 M$_\odot$ yr^{-1}, resulting in an infrared luminosity L_{IR} of 1.25×10^{11} L$_\odot$, well above the threshold for so-called luminous infrared galaxies (LIRGs). The SF rate was undoubtedly higher in the past as the best-fitting decay time-scale τ is around 100 Myr. Such an exponentially decaying SF rate can easily boost the past L_{IR} into the category of ultraluminous infrared galaxies (ULIRGs).

We find that the most luminous star-forming early-type galaxy detected by the *Spitzer Space Telescope* in the SDSS–SWIRE overlap has $L_{FIR} = 5.7$–7.4×10^{10} L$_\odot$ (Sanders & Mirabel 1996) implying a SF rate of 13 M$_\odot$ yr^{-1} based on the relationship of Gao & Solomon (2004). This galaxy is thus just slightly below the cut defining a LIRG of $L_{IR} = 10^{11}$ L$_\odot$ at the time it is observed.

We conclude that the progenitors of the objects we observe on the SF–AGN sequence were most likely ULIRGs. This fits well with the evidence that the local ULIRG population most likely will evolve into intermediate-mass early-type galaxies (Genzel et al. 2001). Dasyra et al. (2006a,b) and Veilleux et al. (2006) have analysed *Hubble Space Telescope* (*HST*) *H*-band imaging and Very Large Telescope (VLT) spectra of low redshift ULRIGs and quasi-stellar objects (QSOs) and concluded that while most of them are ongoing mergers, their kinematic, structural and photometric properties are consistent with them becoming elliptical galaxies and settling on the fundamental plane. Most relevant here is that they find their stellar velocity dispersions to have typical values of around 150 km s^{-1} in overlap with the typical velocity dispersions of our active galaxies that mark the transformation process from blue cloud to red sequence.

The appearance of an AGN phase several hundred Myr after the U/LIRG phase may explain why most local ULIRGs do not appear to contain a luminous AGN (Genzel et al. 1998).

6.3.2 Merger as main trigger

The origin of ULIRG activity is thought to be a galaxy merger (e.g. Genzel et al. 2001). This implies that we are possibly seeing a slightly more advanced stage of a gas-rich merger where the morphology has already settled into a spheroid, and the infrared luminosity has already decayed below the LIRG threshold.

Because of our sample selection, all objects discussed here are morphologically early-type galaxies without spiral or disc structure as far as detectable in the SDSS images. Elliptically shaped galaxies with minor morphological perturbations such as tidal features or dust lanes are not excluded. This selection should in principle enable us to investigate the role of morphological disturbance, hence merger and galaxy interaction activity, along the sequence. However, the fraction of disturbed early-type galaxies in our sample is quite small. We have not found any compelling trend between morphological irregularities and SF/nuclear activity, most likely because SDSS imaging does not provide the necessary sensitivity in terms of depth and spatial resolution. Deeper imaging, preferably at higher spatial
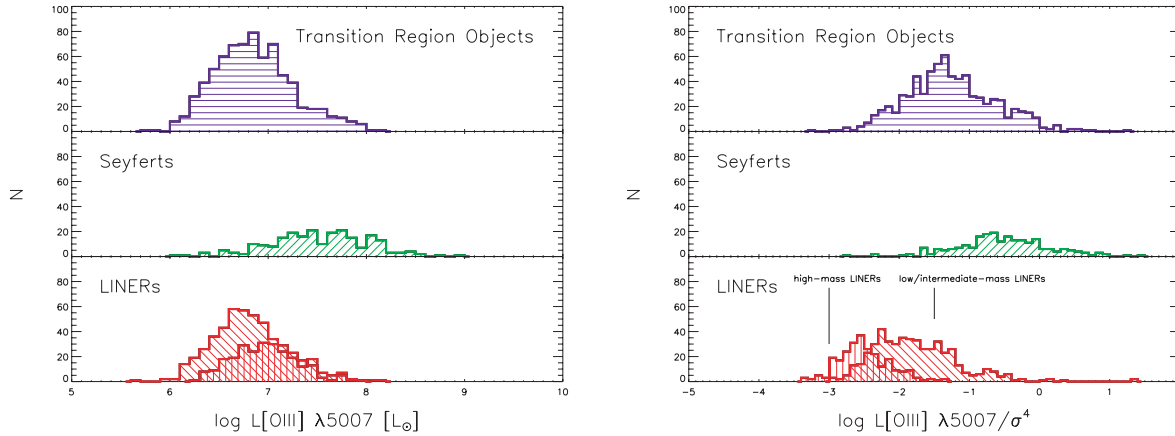
Figure 12. In the left-hand part of this figure, we show the histograms for the L[O III] λ5007 luminosities of our AGN and transition region objects. [O III] is a tracer of the accretion rate (Heckman et al. 2004) and so is an upper limit on the accretion rate of the transition region objects. In the left-hand part, we show the histogram of the quantity L[O III]/σ^4, which is proportional to the Eddington ratio (Kewley et al. 2006). In each part, we go along the sequence from early times to late. First, we show the transition region objects, then the Seyferts and then the LINERs. We split the LINERs into two; while the low- and intermediate-mass LINERS and the high-mass LINERs have similar [O III] luminosities, their Eddington ratios are very different. The low/intermediate-mass LINERs form the low luminosity and high Eddington ratio end of the Seyfert distribution, as would be expected from their place in the time sequence. The high-mass LINERs have Eddington ratios an order of magnitude below their lower mass counterparts. Along the sequence, both absolute L[O III] and Eddington ratio rise, peak and then decline over the time domain covered by the time sequence.

resolution, is clearly needed to identify signatures of recent merger activity in our sample objects (see e.g. van Dokkum 2005; Bell et al. 2006).

6.4 Eddington ratios along the sequence

In the following we discuss the nature of accretion on to the supermassive black hole along the AGN feedback sequence. In Fig. 12, we show the distributions of [O III] luminosity and the quantity L[O III]/σ^4 for Seyfert, low-mass and high-mass LINERS. L[O III]/σ^4 has been introduced by Kewley et al. (2006) as a tracer of the Eddington ratio assuming that [O III] luminosity scales with the AGN bolometric luminosity (Heckman et al. 2004), and that σ^4 provides an estimate of the central supermassive black hole mass (Ferrarese & Merritt 2000; Gebhardt et al. 2000). Based on this quantity Kewley et al. (2006) show that the fundamental difference between Seyferts and LINERs in the SDSS data base is the accretion efficiency, with the LINERs being at lower Eddington ratios than the Seyferts. Since the transition region objects [O III] line luminosities have some contribution from SF, we can treat them as upper limits on both the accretion rate and efficiency.

We find that the Seyfert early types in our sample are high-luminosity AGN with high L[O III] luminosities and high L[O III]/σ^4 ratios, indicating that they are strongly accreting systems relatively close to the Eddington limit. The LINERs, instead, have lower L[O III] luminosities and lower Eddington ratios. There is an interesting trend with mass, however. The massive LINERs exhibit the lowest accretion rates, while the low- and intermediate-mass objects are found between massive LINERs and Seyferts. Hence our low-mass and high-mass LINER early-type galaxies are objects in different states of nuclear activity. The former represent probably the end stage of the SF–AGN sequence. If the Seyfert phase is a high-accretion phase during which the AGN feedback process occurs, then the transition to the LINER phase is the point at which the supply of gas has been largely used up by SF and/or accretion on to the black hole. The massive LINERS characterized by low

Eddington ratios, instead, might be responsible (or at least part of) the rigorous AGN feedback process in massive early-type galaxies that avoid rejuvenation in the first place. Fig. 12 illustrates the extended rise and decline in both accretion rate and Eddington ratio over the time domain covered by the time sequence. While the transition region to Seyfert evolution brings with it an increase in accretion, the progression to a LINER is accompanied by a decline.

6.5 The role of LINERs

Fig. 9 shows that the fraction of LINERs observed increases with increasing galaxy mass, while the fraction of galaxies undergoing the SF–AGN sequence decreases. Hence, LINERs appear to come in two flavours. Some are part of the evolutionary sequence of low- and intermediate-mass galaxies, but the majority is found in the massive, quiescent early-type galaxies of our sample.

It should be emphasized that the LINER-like emission observed here is most likely caused by nuclear activity. The extended LINER-like emission not associated with an AGN found by Sarzi et al. (2006) in very nearby early-type galaxies is significantly weaker (typically with total L[O III] $< 10^6$ L$_\odot$; cf. Fig. 12) and would remain undetected in our sample.

6.5.1 LINERs in low and intermediate masses

As discussed in the previous sections, the early-type galaxies with LINER emission appear on the evolutionary sequence of low- and intermediate-mass objects between Seyfert-like nuclear activity and quiescence. This means that early-type galaxies transition from a high-accretion regime characterized by Seyfert emission to a low accretion regime characterized by LINER emission (Kewley et al. 2006) as they proceed to fade on to the red sequence. This can be interpreted as the AGN running out of fuel. This is well consistent with the study of Yan et al. (2006), who find that many post-starburst galaxies show strong [O II] emission, but no Hα, indicating no further ongoing SF, which they associate with LINERs.

6.5.2 LINERs in massive galaxies

Already in the intermediate-mass bin, most LINERs appear to be associated with stellar quiescence (Fig. 9), and none of the LINERs in the highest mass bin are connected with rejuvenation. This might be AGN feedback in its most rigorous form and is consistent with the fact that the efficiency of AGN feedback must increase with increasing galaxy mass in the models in order to reproduce observed UV colours (Schawinski et al. 2006a). While late SF seems to be terminated by nuclear activity in low-mass early-type galaxies, the AGN in massive galaxies may prevent SF in the first place. These massive galaxies most likely have experienced strong AGN feedback at high accretion nuclear activity at earlier epochs. Indeed, observational evidence for the existence of this process has recently been found (Daddi et al. 2007; Kriek et al. 2007; Rodighiero et al. 2007a).

This LINER-like activity may play the crucial role in maintaining an atmosphere of hot X-ray emitting gas which can shield the galaxy from gas accretion and cooling and so prevent any further SF as suggested by Binney (2004). Such hot gas may then trigger extended LINER-like emission via thermal conduction of self-irradiation as has been seen in massive nearby elliptical galaxies (see e.g. Sarzi et al. 2007 and references therein), although it is likely that the majority of the LINER emission in our sample is associated with (more luminous) nuclear activity.

6.5.3 Misclassified LINERs

We note that some transition region early types are found in the highest mass bin, which show no evidence for a SF episode (see Fig. 9). These transition region objects, being the result of a combination of SF and AGN activity, have no corresponding star forming or Seyferts at the same mass and do not seem to take part in the AGN–SF time sequence. Instead, their properties are far more similar to those of high-mass LINERs. The most likely explanation for this apparent contradiction is that the extreme starburst line of Kewley et al. (2001) led to the misclassification of some LINERs as transition region objects. An improved classification scheme including the low-ionization lines may help here but is beyond the scope of this paper.

6.6 Follow-up observations

The sample presented in this paper is the ideal laboratory for more detailed follow-up studies of the link between SF and nuclear activity in early-type galaxies. Multiwavelength data will tighten constraints on the formation histories, the SF activities, dust contents, central black hole activities and accretion rates of our sample galaxies. This will provide deeper insight into the physics involved.

By observing CO molecular transitions the fate of the molecular gas can be explored. Such observations clarify whether it is really the feedback from AGN that quenches SF, or whether this decline in SF is caused by the fuel supply being exhausted by SF itself. High-resolution radio-continuum observations at different frequencies provide important clues on the relative contributions of SF and the AGN along the sequence. The relative importance and interaction between AGN and SF in the galaxies along our timeline can be further addressed by the analysis of the full SED in the mid-infrared wavelength regime. Mid-infrared imaging helps to pin down the relative amounts of cold, warm and hot dust, while spectroscopy

can disentangle contributions from polycyclic aromatic hydrocarbon (PAH) lines to any hotter dust components due to an AGN. Finally, deep optical imaging would be very valuable and help to determine the role of mergers and interactions along the AGN feedback sequence.

Observations at the observatory of the Institut de Radioastronomie Milimetrique (IRAM) and at the Very Large Array (VLA) to address part of these questions have been taken in 2007 June and July.

7 CONCLUSIONS

We study the relationship between SF and nuclear activity in early-type galaxies at recent epochs. The principle aim is to test whether AGN feedback occurs in these objects, as invoked in most recent models of hierarchical galaxy formation.

For this purpose, we analyse a magnitude-limited sample of 48 023 galaxies drawn from the SDSS DR4 in the redshift range of 0.05 to 0.1 limited to $r < 16.8$. We visually inspected all galaxies in this sample identifying 15 729 morphological early-type galaxies. This paper is the first of a project called MOSES. A detailed description of the catalogue can be found in a companion paper (Schawinski et al., in preparation). Most importantly, the MOSES sample is not biased against SF and nuclear activity thanks to the purely morphological selection criterion. The SDSS photometry is matched to a number of other surveys, namely GALEX, 2MASS and SWIRE, yielding a wavelength coverage from the far-UV to mid-IR. Re-analysing the SDSS spectra, we measure emission-line fluxes, stellar absorption line indices and velocity dispersions. The contributions of the stellar continuum and of the ionized-gas emission to the observed galaxy spectrum are separated by fitting simultaneously stellar population templates.

18.4 per cent of the early-type galaxies in our sample show emission lines, and we employ emission-line ratio (BPT) diagrams to classify them into star forming, AGN–SF composites, Seyfert AGN and LINERs. The fraction of emission-line galaxies increases with decreasing galaxy mass to 40 per cent at the low-mass end ($\sigma < 100\,\mathrm{km\,s^{-1}}$). The emission-line classes are roughly evenly distributed between SF and AGN at intermediate ($100 < \sigma \leqslant 200\,\mathrm{km\,s^{-1}}$) and low ($\sigma \leqslant 100\,\mathrm{km\,s^{-1}}$) masses. At high masses ($\sigma > 200\,\mathrm{km\,s^{-1}}$), instead, only LINER-like emission is detected. The Hα SF rates of those objects classified as currently star-forming range from 0.1 to 25 $M_\odot\,\mathrm{yr^{-1}}$.

We find that the objects with emission are offset from the red sequence and form a well-defined pattern in the colour–σ diagram. Star-forming early-types inhabit the blue cloud, while early-types with AGN (Seyfert and LINER) are located considerably closer to and almost on the red sequence. SF–AGN composites are found right between these two extremes. There is a sequence between the blue cloud and the red sequence from star forming via transition region and Seyfert AGN and LINER to quiescence.

To analyse this transition in more detail, we have developed a method for deriving SF histories with particular focus on quantifying the epoch and mass fraction of the last significant episode of SF. Novel about our approach is to use a combination of UV-optical-NIR photometry and stellar absorption indices as observational constraints.

We find that low- and intermediate-mass early-type galaxies with emission lines have experienced an episode of SF less than ~1 Gyr ago involving 1–10 per cent of their total stellar mass. This recent starburst is best modelled by a steeply declining exponential with e-folding time-scale around 100 Myr. Most importantly, this

time-scale and the mass fraction involved is the same for all the emission line early-type galaxies whether they are star forming, transition region, Seyferts or LINERs. They are offset in time, however, with the star forming being the youngest, and the Seyfert/LINERs being the oldest. Quiescent galaxies (objects without emission lines) have starburst ages larger than 1 Gyr, which sets the time-scale for the transition process we observe. The duration of the various phases along this sequence agree reasonably well with the number fractions observed, once geometric effects of Seyfert activity are taken into account. Dust content decreases along the sequence with highest dust attenuation in the star-forming objects ($E(B - V) \sim 0.1$) and the lowest in the quiescent ones ($E(B - V) \lesssim 0.05$).

These results lead to the conclusion that we are observing an evolutionary sequence and are witnessing the transformation of early-type galaxies from SF via AGN to quiescence. Along this sequence, nuclear activity rises while SF fades. We discuss that gas exhaustion or self-regulation of SF alone does not suffice to explain this fading, which leads to the conclusion that we have detected a sequence in which nuclear activity suppresses SF. We are seeing AGN feedback in action, while low- and intermediate-mass early-type galaxies transition from the blue cloud through the green valley, characterized by nuclear activity, on to the red sequence. The high-mass galaxies in our sample, instead, did not go through this transition in the recent past. These objects have only LINER-like emission and are not associated with rejuvenation. This indicates that the AGN in massive galaxies may prevent SF in the first place, which would be AGN feedback in its most rigorous form.

To conclude, we have found empirical evidence for the occurrence of AGN feedback in early-type galaxies at recent epochs. The galaxy sample presented here is the ideal laboratory for testing more detailed physics of this process. A first important hint from this work is that there is a substantial delay between fading of SF and rise of the AGN by a few hundred Myr. This implies that AGN feedback is not well approximated with an immediate truncation as implicitly assumed in current models.

REFERENCES

Adelman-McCarthy J. K. et al., 2006, ApJS, 162, 38
Allen C. W., 1976, Astrophysical Quantities, 3rd edn. Athlone Press, London
Baldwin J. A., Phillips M. M., Terlevich R., 1981, PASP, 93, 5 (BPT)
Bell E. F. et al., 2006, ApJ, 640, 241
Bennett C. L. et al., 2003, ApJS, 148, 1
Benson A. J., Bower R. G., Frenk C. S., Lacey C. G., Baugh C. M., Cole S., 2003, ApJ, 599, 38
Bernardi M. et al., 2003a, AJ, 125, 1817
Bernardi M. et al., 2003b, AJ, 125, 1849
Bernardi M. et al., 2003c, AJ, 125, 1866
Bernardi M. et al., 2003d, AJ, 125, 1882
Bernardi M., Nichol R. C., Sheth R. K., Miller C. J., Brinkmann J., 2006, AJ, 131, 1288
Best P. N., Kauffmann G., Heckman T. M., Brinchmann J., Charlot S., Ivezić Ž., White S. D. M., 2005, MNRAS, 362, 25
Best P. N., Kaiser C. R., Heckman T. M., Kauffmann G., 2006, MNRAS, 368, L67
Binney J., 2004, MNRAS, 347, 1093
Birnboim Y., Dekel A., Neistein E., 2007, MNRAS, 380, 339
Blanton M. R., Lin H., Lupton R. H., Maley F. M., Young N., Zehavi I., Loveday J., 2003a, AJ, 125, 2276
Blanton M. R. et al., 2003b, AJ, 125, 2348
Blanton M. R. et al., 2005, AJ, 129, 2562
Bouchet P., Lequeux J., Maurice E., Prevot L., Prevot-Burnichon M. L., 1985, A&A, 149, 330
Bower R. G., Benson A. J., Malbon R., Helly J. C., Frenk C. S., Baugh C. M., Cole S., Lacey C. G., 2006, MNRAS, 370, 645
Caldwell N., Rose J. A., Concannon K. D., 2003, AJ, 125, 2891
Calzetti D., Armus L., Bohlin R. C., Kinney A. L., Koornneef J., Storchi-Bergmann T., 2000, ApJ, 533, 682
Cappellari M., Emsellem E., 2004, PASP, 116, 138
Carson D., 2007, PhD thesis, Univ. Portsmouth
Cattaneo A., Dekel A., Devriendt J., Guiderdoni B., Blaizot J., 2006, MNRAS, 370, 1651
Cattaneo A. et al., 2007, MNRAS, 377, 63
Cavaliere A., Menci N., 2007, ApJ, 664, 47
Cimatti A., Daddi E., Renzini A., 2006, A&A, 453, L29
Ciotti L., Ostriker J. P., 1997, ApJ, 487, L105
Combes F., Young L. M., Bureau M., 2007, MNRAS, 337, 1795
Connolly A. J., Szalay A. S., 1999, AJ, 117, 2052
Croton D. J. et al., 2006, MNRAS, 365, 11
Daddi E. et al., 2007, preprint (arXiv:0705.2831)
Dasyra K. M. et al., 2006a, ApJ, 638, 745
Dasyra K. M. et al., 2006b, ApJ, 651, 835
Davies R., Mueller Sanchez F., Genzel R., Tacconi L., Hicks E., Friedrich S., Sternberg A., 2007, ApJ, in press (arXiv:0704.1374)
Dekel A., Silk J., 1986, ApJ, 303, 39
De Lucia G., Springel V., White S. D. M., Croton D., Kauffmann G., 2006, MNRAS, 366, 499
Di Matteo T., Springel V., Hernquist L., 2005, Nat, 433, 604
Di Matteo T., Colberg J., Springel V., Hernquist L., Sijacki D., 2007, preprint (arXiv:0705.2269)
Eisenstein D. J. et al., 2001, AJ, 122, 2267
Faber S. M. et al., 2007, ApJ, 665, 265
Fabian A. C., Sanders J. S., Taylor G. B., Allen S. W., 2005, MNRAS, 360, L20

Fabian A. C., Sanders J. S., Taylor G. B., Allen S. W., Crawford C. S., Johnstone R. M., Iwasawa K., 2006, MNRAS, 366, 417
Ferrarese L., Merritt D., 2000, ApJ, 539, L9
Ferreras I., Silk J., 2000, ApJ, 541, L37
Fitzpatrick E. L., 1986, AJ, 92, 1068
Fukugita M., Ichikawa T., Gunn J. E., Doi M., Shimasaku K., Schneider D. P., 1996, AJ, 111, 1748
Fukugita M., Nakamura O., Turner E. L., Helmboldt J., Nichol R. C., 2004, ApJ, 601, L127
Fukugita M. et al., 2007, AJ, 134, 579
Gao Y., Solomon P. M., 2004, ApJ, 606, 271
Gebhardt K. et al., 2000, ApJ, 539, L13
Genzel R. et al., 1998, ApJ, 498, 579
Genzel R., Tacconi L. J., Rigopoulou D., Lutz D., Tecza M., 2001, ApJ, 563, 527
Granato G. L., Silva L., Monaco P., Panuzzo P., Salucci P., De Zotti G., Danese L., 2001, MNRAS, 324, 757
Granato G. L., De Zotti G., Silva L., Bressan A., Danese L., 2004, ApJ, 600, 580
Graves G. J., Faber S. M., Schiavon R. P., Yan R., 2007, preprint (arXiv:0707.1523)
Gunn J. E. et al., 1998, AJ, 116, 3040
Harris G. L. H., Harris W. E., 2000, AJ, 120, 2423
Harris W. E., Harris G. L. H., 2002, AJ, 123, 3108
Harris G. L. H., Harris W. E., Poole G. B., 1999, AJ, 117, 855
Heckman T. M., Kauffmann G., Brinchmann J., Charlot S., Tremonti C., White S. D. M., 2004, ApJ, 613, 109
Hopkins P. F., Cox T. J., Keres D., Hernquist L., 2007, preprint (arXiv:0707.1523)
Jimenez R., Bernardi M., Haiman Z., Panter B., Heavens A. F., 2006, preprint (astro-ph/0670724)
Kauffmann G., Charlot S., 1998, MNRAS, 294, 705
Kauffmann G., Colberg J. M., Diaferio A., White S. D. M., 1999, MNRAS, 303, 188
Kauffmann G. et al., 2003, MNRAS, 346, 1055
Kauffmann G. et al., 2007, ApJS, in press (astro-ph/0609436)
Kaviraj S., Devriendt J. E. G., Ferreras I., Yi S. K., 2005, MNRAS, 360, 60
Kaviraj S. et al., 2007, ApJS, in press (astro-ph/0601029)
Kawata D., Gibson B. K., 2005, MNRAS, 358, L16
Kennicutt R. C., Jr, 1998, ApJ, 498, 541
Kewley L. J., Dopita M. A., Sutherland R. S., Heisler C. A., Trevena J., 2001, ApJ, 556, 121
Kewley L. J., Groves B., Kauffmann G., Heckman T., 2006, MNRAS, 372, 961
Khochfar S., Ostriker J. P., 2007, preprint (arXiv:0704.2418)
Kriek M. et al., 2007, ApJ, in press (astro-ph/0611724)
Lonsdale C. J. et al., 2003, PASP, 115, 897
MacArthur L. A., 2005, ApJ, 623, 795
Maraston C., 1998, MNRAS, 300, 872
Maraston C., 2005, MNRAS, 362, 799
Maraston C., Thomas D., 2000, ApJ, 541, 126
Martin D. C. et al., 2005, ApJ, 619, L1
Martin D. C. et al., 2007, in press (astro-ph/0703281)
Morganti R. et al., 2006, MNRAS, 371, 157
Nagashima M., Lacey C. G., Okamoto T., Baugh C. M., Frenk C. S., Cole S., 2005, MNRAS, 363, L31

Nandra K. et al., 2007, ApJ, 660, L11
Nelan J. E., Smith R. J., Hudson M. J., Wegner G. A., Lucey J. R., Moore S. A. W., Quinney S. J., Suntzeff N. B., 2005, ApJ, 632, 137
Panter B., Heavens A. F., Jimenez R., 2003, MNRAS, 343, 1145
Panter B., Jimenez R., Heavens A. F., Charlot S., 2007, MNRAS, 378, 1550
Prevot M. L., Lequeux J., Prevot L., Maurice E., Rocca-Volmerange B., 1984, A&A, 132, 389
Rodighiero G. et al., 2007a, MNRAS, 376, 416
Rodighiero G., Cimatti A., Franceschini A., Brusa M., Fritz J., Bolzonella M., 2007b, A&A, 470, 21
Salim S. et al., 2007, ApJS, in press (arXiv:0704.3611)
Sanders D. B., Mirabel I. F., 1996, ARA&A, 34, 749
Sarajedini A., Jablonka P., 2005, AJ, 130, 1627
Sarzi M. et al., 2006, MNRAS, 366, 1151
Sarzi M. et al., 2007, New Astron. Rev., 51, 18
Schawinski K. et al., 2006a, Nat, 442, 888
Schawinski K. et al., 2006b, ApJS, in press (astro-ph/0601036)
Schmidt M., 1959, ApJ, 129, 243
Sijacki D., Springel V., Di Matteo T., Hernquist L., 2007, MNRAS, 380, 877
Silk J., 2005, MNRAS, 364, 1337
Silk J., Rees M. J., 1998, A&A, 331, L1
Skrutskie M. F. et al., 2006, AJ, 131, 1163
Springel V., White S. D. M., Tormen G., Kauffmann G., 2001, MNRAS, 328, 726
Springel V., Di Matteo T., Hernquist L., 2005a, MNRAS, 361, 776
Springel V. et al., 2005b, Nat, 435, 629
Stasińska G., Cid Fernandes R., Mateus A., Sodré L., Asari N. V., 2006, MNRAS, 371, 972
Stoughton C. et al., 2002, AJ, 123, 485
Sutherland R. S., Dopita M. A., 1993, ApJS, 88, 253
Thomas D., 1999, MNRAS, 306, 655
Thomas D., Maraston C., Bender R., 2003, MNRAS, 339, 897
Thomas D., Maraston C., Korn A., 2004, MNRAS, 351, L19
Thomas D., Maraston C., Bender R., Mendes de Oliveira C., 2005, ApJ, 621, 673
Trager S. C., Worthey G., Faber S. M., Burstein D., Gonzalez J. J., 1998, ApJS, 116, 1
Trager S. C., Faber S. M., Worthey G., González J. J., 2000, AJ, 120, 165
Tremonti C. A. et al., 2004, ApJ, 613, 898
van Dokkum P. G., 2005, AJ, 130, 2647
Veilleux S. et al., 2006, ApJ, 643, 707
Wake D. A. et al., 2006, MNRAS, 372, 537
White S. D. M., Frenk C. S., 1991, ApJ, 379, 52
Wild V., Kauffmann G., Heckman T., Charlot S., Lemson G., Brinchmann J., Reichard T., Pasquali A., 2007, MNRAS, 381, 543
Worthey G., Ottaviani D. L., 1997, ApJS, 111, 377
Worthey G., Faber S. M., Gonzalez J. J., Burstein D., 1994, ApJS, 94, 687
Yan R., Newman J. A., Faber S. M., Konidaris N., Koo D., Davis M., 2006, ApJ, 648, 281
Yi S. K. et al., 2005, ApJ, 619, L111
York D. G. et al., 2000, AJ, 120, 1579
Young L. M., 2002, AJ, 124, 788

This paper has been typeset from a TEX/LATEX file prepared by the author.